

Penetration performance of axisymmetric U-shape-nose grooved projectile into aluminum target: Theoretical model and experiment

Abstract

The penetration performance of projectiles is closely related to their nose shape as it influences the kinetic energy penetration of a rigid projectile. One new type of projectile, which is entitled U-shape-nose grooved projectile, is introduced in this study. A theoretical model, which describes the structural characterization of U-shape-nose grooved projectile, is constructed here to investigate the penetration characters into an aluminum target. Moreover, comparative penetration experiments were conducted to investigate the penetration performance of U-shape-nose grooved projectile. Effects of characteristic parameters and shape optimal conditions of the U-shape-nose grooved projectile on the penetration performance are analyzed with the theoretical model validated by the experimental results. It has been proved that U-shape-nose grooved projectile has a more excellent penetration performance than the ogive-nose projectile based on comparison between the results of experimental and theoretical model. The projectile with U-shape-nose grooves sharpens the nose of the projectile and changes the failure mode of target during penetration, which has advantages of decreasing penetration resistance and enhancing the depth of penetration.

Keywords

Penetration; U-shape-nose grooved projectile; Aluminum target; Localized interaction models; Depth of penetration (DOP).

Jiajie Deng ^a
 Xianfeng Zhang ^{a*}
 Chuang Liu ^a
 Wenjie Wang ^a

^a School of Mechanical Engineering, Nanjing University of Science & Technology, Nanjing 210094, P.R. China, E-mail: jiajie_0827@163.com, lynx@njust.edu.cn, lc9009njust@163.com, wwj0704@126.com

* Corresponding author

<http://dx.doi.org/10.1590/1679-78254511>

Received September 09, 2017
 In revised form December 01, 2017
 Accepted January 26, 2018
 Available online February 02, 2018

1 INTRODUCTION

Earth penetration weapons (EPW), as an effective means of attacking hard and deeply buried target, have attracted lots of attention and undergone a rapid development. The penetrator structure should be kept integral until the prospective depth of penetration is achieved in order to improve the penetration performance. However, the buried depth of the underground fortifications significantly increases nowadays on the other hand. The improvement of depth of penetration is the currently subject of considerable researches. The penetration performance of an EPW is commonly enhanced by two approaches, namely, optimizing the penetrator structure and increasing the impact velocity. Based on the research on the expanded metal tubes subjected to impact loads (Hatami and Nouri, 2015; Hatami et al., 2017; Jahromi and Hatami, 2017; Nouri et al., 2015; Nouri and Hatami, 2017), the energy absorption performance of the expanded metal tubes was controlled by their structure. Likewise, increasing the kinetic energy of penetrator per unit cross section area is an effective way to increase the depth of penetration (DOP) by optimizing the structure of the penetrator. Compared with the ogive-nose projectile, the conical projectile possesses much higher kinetic energy per unit cross section area on the surface while the conical-nose shape has a low-quality utilization ratio in practical engineering application. Therefore, it is significant to design a projectile incorporating the advantage of the ogive-nose projectile and conical-nose projectile to achieve relatively excellent penetration performance with high-quality utilization ratio.

Penetration of the projectile of revolution into semi-infinite target has been extensively studied for a long time. The substantial efforts have been made by systematic theoretical investigations in order to understand the mechanism of targets impacted by projectiles. From the viewpoint of the penetration experiments and pertinent mechanics, Luk and Forrestal (1987), Forrestal et al. (1994) and Forrestal and Warren (2008) presented a semi-empirical equation based on the cavity expansion theory to estimate the penetration resistance of ogive-nose projectile into ductile metal and concrete. Yankelevsky and Adin (1980), Yankelevsky (1997) and Li et al. (2000) proposed a disk model to analyze the penetration resistance of the ogive-nose projectile. Based on the disk model,

Jones and Rule (2000) obtained a related dimensionless constant, namely the nose shape coefficient, and determined its relationship to the inertial resistance. Chen and Li (2002), Li and Chen (2003), and Zhao et al. (2003) analyzed the coefficient with different nose shapes and the relationship between the nose shape coefficient and the velocity, respectively. Based on the previously developed localized interaction models (LIMs) proposed by Dubinskii (1995), Ben-Dor et al. (1996) introduced a generalized formula for the penetration of arbitrary projectile of revolution to calculate the resistance and the ultimate depth of penetration.

Considerable research has been conducted to study the influence on the nose shape structure of the projectile and the optimization of nose shape. Yankelevsky and Gluck (1980) presented an optimal shape by minimizing the instantaneous resistance of the proposed disk model, which was determined by using a single parameter relevant to the velocity, overload and target properties. Based on the cavity expansion theory, an optimized double-ogive-nose projectile, combined with a low penetration resistance, was proposed by Liu et al. (2014, 2015) to analyze the dependency relationship between the nose shape coefficient and the double-ogive-nose projectile. Based on the LIMs, Ben-Dor et al. (1996, 2009) determined the optimized shape of typical projectiles of revolution penetrating into semi-infinite to maximize the depth of penetration. The irregular nose head projectile was introduced and its penetration performance was investigated by experimental and theoretical methods (Mayersak, 2003; Chai, 2014). The results indicated that the irregular nose head projectile made higher depth of penetration than the traditional ogive-nose projectile. For the projectiles of revolution, the improvement of penetration performance is limited by the nose shapes. Thus researchers began to pay attention to the geometry design and penetration mechanics of the projectile with non-circular cross section structure. Ragnedda and Serra (2010) introduced a projectile with non-axisymmetric shape nose, which called screwdriver shape. According to the theoretical calculation, the projectile with non-axisymmetric shape nose showed the higher penetration depth than axisymmetric projectile. Yakunina (2001, 2005) and Yakunna (2005) proposed a design method based on the LIMs and obtained the projectile with cylindrical shank and the optimal 3D-nose shape, which has a better penetration performance. Fan et al. (2013) analyzed the resistance of projectile with spiral grooves and determined the advantage of increasing the depth of penetration by experiment and numerical simulation. Erengil and Cargile (2002) designed a new type of projectile with ogive-nose and circular-truncated-cone shank, which is named concept projectile for high-speed penetration (CPHP). The available experimental results prove that CPHP possesses excellent penetration capability at higher striking velocities (He et al., 2016; Wu et al., 2008). Moreover, the structure stability and penetration performance of CPHP is related to the projectile material (Erengil and Cargile, 2002; Wu et al., 2008; Liang et al., 2008). Zhang et al. (2014), Zhang (2016) and Zhang et al. (2016) studied the trajectory stability, dynamic structure response and mechanical model of grooved-tapered projectiles. Zhang et al. (2017) conducted high velocity penetration experiments using ogive-nose, double-ogive-nose and grooved-tapered projectile and proposed a crater depth model based on the test results. The analysis result shows that double-ogive-nose projectile has higher penetration ability and the grooved-tapered projectile has better trajectory stability. Pang et al. (2015a, 2015b) and Guo et al. (2015) proposed the structures of the projectiles with the axisymmetric and non-axisymmetric nose grooves. The available experiment and simulation results preliminarily proved the excellent penetration performance of the projectiles with the axisymmetric and non-axisymmetric nose grooves. However, studies on the penetration mechanics of the projectile with grooves were mainly investigated by experiments and numerical simulations, while theoretical works mainly focused on the optimization of the projectile. Only a limited amount of research has been conducted on the penetration dynamic model of projectile with grooves nose.

A new concept projectile, which is named as U-shape-nose grooved projectile with axisymmetric grooves nose, is introduced in the present manuscript. The geometric structure of U-shape-nose grooved projectile is characterized in the cylindrical coordinate system. Based on the LIMs and discretization model, a theoretical model is proposed to investigate the depth of penetration and the penetration process of U-shape-nose grooved projectile into an aluminum target. Comparative penetration tests are conducted with moderate to low impact velocity range for providing insight into the penetration performance. By comparing with the experimental DOP, the validity of the proposed theoretical model is verified. Furthermore, the penetration process and the influence of the characteristic parameters of the U-shape-nose grooved projectile on the penetration performance are analyzed. The theoretical and experimental results prove that the U-shape-nose grooved projectile has a more excellent penetration performance. The theoretical analytical model can predict the DOP of U-shape-nose grooved projectile into ductile metal target.

2 THEORETICAL MODEL OF PENETRATION FOR U-SHAPE-NOSE GROOVED PROJECTILE

2.1 Structural characterization

It could be concluded from the previous research (Pang et al., 2015a, 2015b) that nose grooves could improve the penetration capability to damage targets, through reducing the contact area. In the present research, the projectile is ogive-nose projectile with several grooves distributed evenly in the nose. As shown in Figure 1, each groove is machined by a cylinder milling cutter. In the process of milling groove, the cylinder milling cutter cuts the nose of projectile with its cutting rotational speed of ω_{cutter} . Meanwhile the cylinder milling cutter moves from the tip of the projectile nose to the projectile shank surface at a certain cutting speed of v_{cutter} and a groove forms. Taking the example of the projectile with four grooves (Figure 2), the geometry of the projectile nose could be depicted as four groove arc surfaces inside and four isolated ogive arc surfaces attached outside. This type of projectile can be considered as a kind of non-circular cross-sectional nose of the projectile. According to the cross section of the projectile nose in Figure 2, the groove presents the symmetrical U-shape outline. Therefore, this type of projectile is defined as the U-shape-nose grooved projectile.



Figure 1: Manufacturing process of U-shape-nose grooved projectile

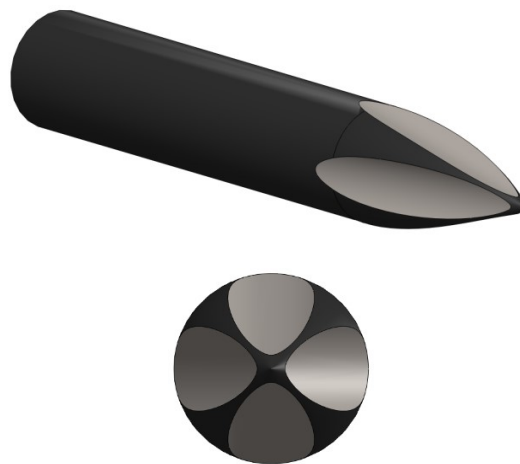


Figure 2: Three-dimensional diagram of U-shape-nose grooved projectile

In order to specifically illustrate the geometry of the projectile, the corresponding characteristic parameters in Cartesian coordinates (OXY) are labeled in Figure 3. The nose is comprised of a partial ogive and several grooved surfaces. The radius of the projectile is r_p . The length and the radius of the ogive-nose are b and S_r , respectively. The equation of the lateral surface of the partial ogive of the projectile $f_o(x)$ can be uniformly described as:

$$f_o(x) = \begin{cases} (r_p - S_r) + \sqrt{S_r^2 - (x - b)^2} & 0 < x \leq b \\ r & x > b \end{cases} \quad (1)$$

Specifically, four characteristic parameters are defined to represent the geometry variation of U-shape-nose grooved projectile, i.e. x_0 , α , R_u and n . As shown in Figure 3, x_0 is the X-coordinate value of the initial groove position, while distance of x_0 is the initial position of the U-shape groove shifted towards the projectile tip. n is the number of the groove. The axis of the cylinder milling cutter is parallel to the direction of EF and the radius of the cutter is R_u , as well as the radius of U-shape-nose groove. The angle of U-shape-nose groove between the direction of EF and X axis is α . The length of groove L_u on the X-axis is given as follows:

$$L_u = f_o(x_0) / \tan \alpha \tag{2}$$

Grooves are distributed evenly in the nose of the projectile. Due to the symmetry of U-shape-nose grooved projectile, the whole surface of a side section of the projectile can be divided into n equally spaced interval in polar coordinates ($r-\theta$). As for the range of 0 to $2\pi/n$ at a side section of U-shape-nose grooved projectile in Figure 4, LHG encloses the two regions wherein GH represents the region of U-shape grooved arc surface and HL represents the region of remaining ogive-nose arc surface. The points N is the arbitrary points within the region of U-shape grooved arc surface. The polar angle and polar radius are expressed as θ and $f_u(x, \theta)$, respectively. The region of U-shape grooved arc surface is symmetric with respect to OM, in which the radius of the arc surface is $R_u/\cos\alpha$ and the central angle is 2λ . Correspondingly, the central angle of remaining ogive-nose arc surface is $2\pi/n-2\lambda$.

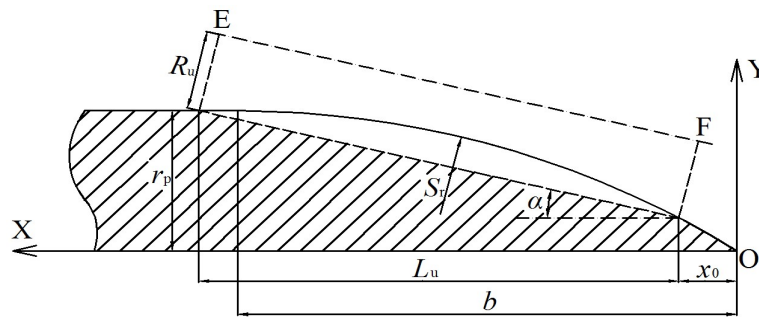


Figure 3: Cross-section of U-shape-nose grooved projectile

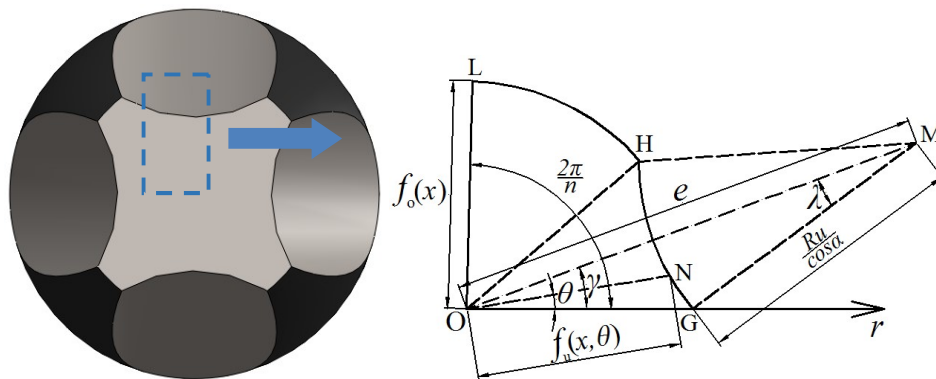


Figure 4: Geometry of $2\pi/n$ ranges at side section of U-shape-nose grooved projectile in polar coordinates

In view of geometric relationship in Figure 3 and Figure 4, the expression of the distance e , which is defined from axis of EF to X-axis at the Y direction, is given by:

$$e = f_o(x_0) + (x - x_0) \tan \alpha + R_u / \cos \alpha \tag{3}$$

Applying the cosine law to the relationship of OGM triangle, the half central angle λ of U-shape grooved arc surface can be expressed as:

$$\lambda = \cos^{-1} \left(\frac{(R_u / \cos \alpha)^2 + e^2 - f_o^2(x)}{2 \cdot e \cdot R_u / \cos \alpha} \right) \tag{4}$$

Thus the half central angle γ of remaining ogive-nose arc surface can be defined by the same method, as:

$$\gamma = \cos^{-1}\left(\frac{f_o^2(x) + e^2 - (R_u/\cos\alpha)^2}{2 \cdot e \cdot f_o(x)}\right) \tag{5}$$

Due to the symmetry of U-shape-nose grooves following periodic characteristic could be found among the lateral outer surface function of the U-shape grooved arc surface $f_u(x, \theta)$ and the ogive-nose arc surface $f_o(x, \theta)$:

$$f_u(x, \theta) = f_u(x, \theta + \frac{2\pi}{n}) \tag{6a}$$

$$f_o(x, \theta) = f_o(x, \theta + \frac{2\pi}{n}) \tag{6b}$$

For the geometry of U-shape-nose, the cosine function, which includes the lateral outer surface function of U-shape grooved arc surface $f_u(x, \theta)$, is derived from the relationship of OMN triangle:

$$\cos|\theta - \gamma| = \frac{f_u^2(x, \theta) + e^2 - (R_u / \cos\alpha)^2}{2 \cdot e \cdot f_u(x, \theta)} \tag{7}$$

where $0 \leq \theta \leq 2\gamma$. By solving the Eq. 7, the lateral outer surface function $f_u(x, \theta)$ of U-shape grooved arc surface is:

$$f_u(x, \theta) = e \cdot \cos|\theta - \gamma| - \sqrt{e^2 \cdot \cos^2|\theta - \gamma| - e^2 + (R_u / \cos\alpha)^2} \tag{8}$$

As shown in Figure 3, the lateral outer surface function $f(x, \theta)$ of the whole U-shape-nose grooved projectile could be divided into three parts in cylindrical coordinates $(x-r-\theta)$.

Part one: $0 \leq x < x_0$, the lateral outer surface is the ogive of projectile from the tip to the initial position of the U-shape groove:

$$f(x, \theta) = f_o(x) \tag{9}$$

Part two: $x_0 \leq x < b$, the lateral outer surface is consist of U-shape grooved surface and remaining ogive-nose surface:

$$f(x, \theta) = \begin{cases} f_u(x, \theta) & \frac{2k\pi}{n} \leq \theta < \frac{2k\pi}{n} + 2\gamma \\ f_o(x) & \frac{2k\pi}{n} + 2\gamma \leq \theta < \frac{(2k+2)\pi}{n} \end{cases} \quad (k = 0, 1, 2, \dots, n-1) \tag{10}$$

Part three: $b \leq x < x_0 + L_u$, the lateral outer surface is consist of U-shape grooved surface and remaining projectile shank surface:

$$f(x, \theta) = \begin{cases} f_u(x, \theta) & \frac{2k\pi}{n} \leq \theta < \frac{2k\pi}{n} + 2\gamma \\ r_p & \frac{2k\pi}{n} + 2\gamma \leq \theta < \frac{(2k+2)\pi}{n} \end{cases} \quad (k = 0, 1, 2, \dots, n-1) \tag{11}$$

Once the characteristic parameters of the U-shape-nose grooved projectile (n, R_u, x_0, α) are determined, the value of θ can be calculated. According to the periodic trend of Eq. 6, the lateral outer surface function $f(x, \theta)$ of the whole U-shape-nose grooved projectile can be obtained by Eq. 9- Eq. 11.

2.2 Penetration depth equations based on the Localized Interaction models (LIMs)

It is well known that the models of cavity expansion in materials have emerged as an essential tool for investigation of impact dynamics. Much more work has been devoted to the problem of cavity expansion in metals. The pioneering work of Bishop et al. (1945) concerning on the spherical and cylindrical cavity expansion analysis, proposed the static and quasi-static expression of metals. Hill (1980) reviewed Bishop’s proposal and presented

the dynamic expansion of the spherical cavity expression for metals. The issue of metal compressibility and strain-hardening was dealt analytically, several years later, by Luk et al. (1991) and Forrestal and Warren (2008). The spherically symmetric, cavity-expansion results of the radial stress σ_r at the cavity surface versus cavity-expansion velocity V for strain-hardening metal can be expressed in the form of:

$$\sigma_r/Y_t = a_0 + a_1 \left(V \cdot \sqrt{Y_t/\rho_t} \right) + a_2 \left(V \cdot \sqrt{Y_t/\rho_t} \right)^2 \tag{12}$$

where Y_t is the yield stress of materials and ρ_t is the density of the target. Coefficients a_0, a_1, a_2 are the resistance coefficients of the metal, which depend only on material properties. For an incompressible material:

$$a_0 = \frac{2}{3} \left[1 + \left(\frac{2E}{3Y_t} \right)^{n_t} I \right], \quad a_1 = 0, \quad a_2 = 3/2 \tag{13a}$$

$$I = \int_0^{1-(3Y_t/2E)} \frac{(-\ln \delta)^{n_t}}{1-\delta} d\delta \tag{13b}$$

where E is the young modulus of the elastic-plastic ductile material. n_t is the strain-hardening exponent of elastic-plastic ductile material. The integration I is derived by Piekutowski et al. (1996).

For the U-shape-nose grooved projectile, the normal stresses depend on the angle between the inner normal and the tangent vectors at a given location on the projectile surface. According to the surface partition of U-shape-nose grooved projectile, the angle in the U-shape grooved surface is a constant and the angle in the remaining ogive-nose surface varies with the position on the nose. Then, the normal stresses σ_n acting on the localized surface of the projectile can be divided into two parts: σ_{nu} and σ_{no} , which are the normal stresses on the U-shape grooved surface and the ogive-nose surface, respectively. Therefore, the specific expression of normal stresses σ_n is defined:

$$\sigma_n = \begin{cases} \sigma_{nu}(v_x, \alpha) & \frac{2k\pi}{n} \leq \theta < \frac{2k\pi}{n} + 2\gamma \\ \sigma_{no}(v_x, \beta) & \frac{2k\pi}{n} + 2\gamma \leq \theta < \frac{(2k+2)\pi}{n} \end{cases} \quad (k = 0, 1, 2, \dots, n-1) \tag{14}$$

where v_x is the velocity of the projectile and β is a parameter that obtained by $\beta = \tan^{-1} f'_o(x)$. From the geometry in Figure 3, the resultant force acting on the contact surface between projectile and target is consist of the force on the U-shape grooved surface and the remaining ogive-nose surface. The elementary force $dF(x, \theta)$ at each cross-section position of projectile nose has the following expression:

$$dF(x, \theta) = \begin{cases} \frac{2}{n} (\pi - \gamma) \cdot f_o(x) \cdot \sigma_n(v_x, \beta) \cdot (\sin \beta + \mu \cos \beta) dx & \frac{2k\pi}{n} \leq \theta < \frac{2k\pi}{n} + 2\gamma \\ \sum_{\theta=0}^{2\gamma} f_u(x, \theta) \cdot \sigma_n(v_x, \alpha) (\sin \alpha + \mu \cos \alpha) dx & \frac{2k\pi}{n} + 2\gamma \leq \theta < \frac{(2k+2)\pi}{n} \end{cases} \tag{15}$$

$(k = 0, 1, 2, \dots, n-1)$

where μ is the coefficient of sliding friction.

If the projectile mass is m , from Newton's second law:

$$\begin{aligned} ma &= -F \\ m(dv_x/dt) &= -F \\ m(dp/dt) \cdot (dv_x/dp) &= -F \\ mv_x(dv_x/dp) &= -F \end{aligned} \tag{16}$$

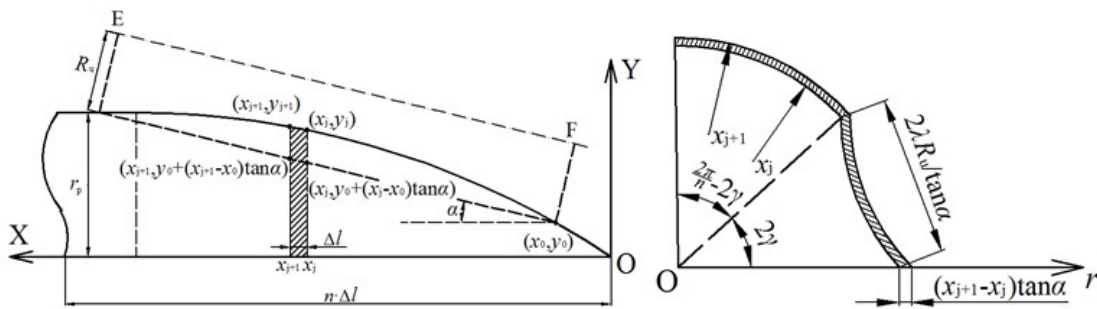
where F, a, v_x and p are the resistance force, deceleration, velocity and displacement of projectile. t is the time. The expression of resistance dF in Eq. 15 along the X-axis, which is the direction of the projectile's movement, is expressed as follows:

$$mv_x(dv_x/dp) = - \int_0^{2\pi} d\theta \int_0^{x_0+L_u} dF(x, \theta) \tag{17}$$

The final penetration depth is obtained by integrating Eq. 16 from v_0 to 0 and 0 to P .

2.3 Prediction with discretization model

In analyzing the penetration process of ductile metal target subjected by U-shape-nose grooved projectile, a discrete 3D model is established to calculate the motion of U-shape-nose grooved projectile, as shown in Figure 5. With the coordinates XOY fixed on the projectile, the projectile is divided into n sticks with each width of stick Δl . The remaining ogive-nose arc surface and U-shape grooved arc surface are divided into a unit circle in r - θ , of which the width are $x_{j+1}-x_j$ and $(x_{j+1}-x_j) \cdot \tan\alpha$, respectively. The subscript j denotes the sequence number in the spatial discretization. Based on the method of discretization model above, the lateral outer surface and the range of 0 to $2\pi/n$ at a side section of U-shape-nose grooved projectile are divided into discretization intervals during the time intervals Δt . The subscript i represents the sequence number of the current time step.



(a) Cross-section of U-shape-nose grooved projectile (b) Side-section of U-shape-nose grooved projectile

Figure 5: Discretization of U-shape-nose grooved projectile

The resistance on the remaining ogive-nose arc surface at the time t^{i+1} can be expressed as:

$$F_o^{i+1} = \sum_j \left\{ \left(\frac{2\pi}{n} - 2\gamma_j^{i+1} \right) \cdot \left[\left(\sigma_{n_o j}^{i+1} + \sigma_{n_o j+1}^{i+1} \right) \left(y_{j+1}^{i+1} - y_j^{i+1} \right)^2 + \mu \left(\sigma_{n_o j}^{i+1} + \sigma_{n_o j+1}^{i+1} \right) \left(y_{j+1}^{i+1} + y_j^{i+1} \right) \left(x_{j+1}^{i+1} - x_j^{i+1} \right) \right] \right\} \tag{18}$$

where, $\sigma_{n_o j}^i$ depends on the time, the current position of the projectile outer surface and the instantaneous velocity $v_{n_o j}^{i+1}$, which is obtained by Eq. 12 and Eq. 13. The tangle angle β_j^{i+1} and normal velocity $v_{n_o j}^{i+1}$ of the j discrete point on the remaining ogive-nose surface at the time t^{i+1} is:

$$\beta_j^{i+1} = \tan^{-1} \left(\frac{y_{j+1}^{i+1} - y_j^{i+1}}{x_{j+1}^{i+1} - x_j^{i+1}} \right) \tag{19}$$

$$v_{n_o j}^{i+1} = v_j^{i+1} \sin \left(\frac{\beta_j^{i+1} + \beta_{j-1}^{i+1}}{2} \right) \tag{20}$$

Meanwhile, the resistance on the U-shape grooved surface of the projectile at the time t^{i+1} can be express as:

$$F_u^{i+1} = \sum_j \left[4\lambda_j^{i+1} \left(\sigma_{n_u j}^{i+1} + \sigma_{n_u j+1}^{i+1} \right) \left(\frac{R_u}{\cos \alpha} \right) \left(x_{j+1}^{i+1} - x_j^{i+1} \right) \left(\mu + \tan \alpha \right) \right] \tag{21}$$

where, $\sigma_{n_u j}^i$ is calculated by the normal stress of U-shape grooved surface in Eq. 13. The normal velocity $v_{n_u j}^{i+1}$ of the j discrete point on U-shape grooved surface at the time t^{i+1} is:

$$v_{nuj}^{i+1} = v_j^{i+1} \sin \alpha \tag{22}$$

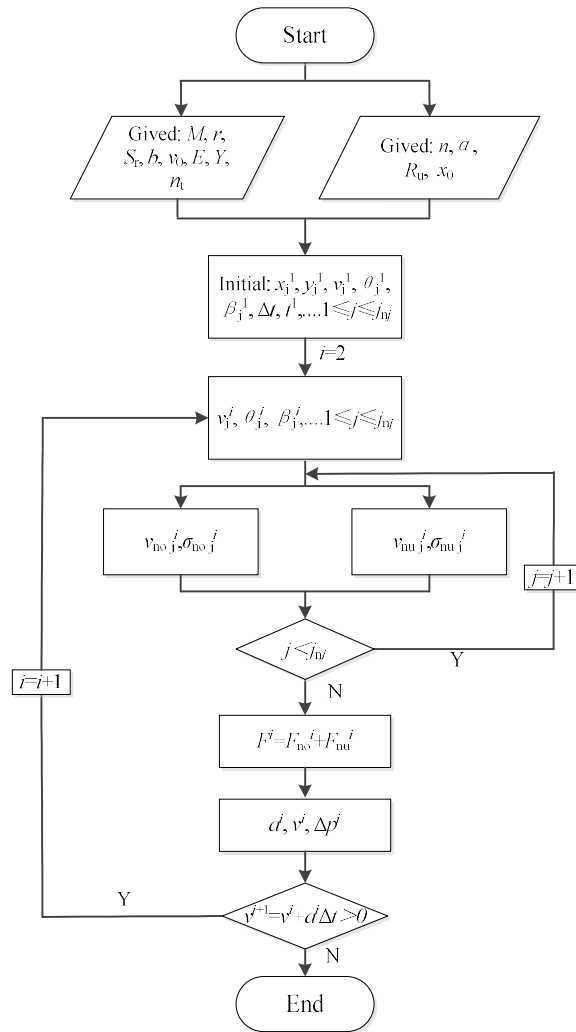


Figure 6: Flow chart of the iterative calculation on the penetration process of U-shape-nose grooved projectile

The resistance on the whole surface of the projectile at the time t^{i+1} can be obtained from Eq. 18 and Eq. 21.

$$F^{i+1} = F_o^{i+1} + F_u^{i+1} = \int_{S_o} (\sigma_{no} \sin \theta + \mu \sigma_{no} \cos \theta) dS + \int_{S_u} (\sigma_{nu} \sin \alpha + \mu \sigma_{nu} \cos \alpha) dS \tag{23}$$

where, S_o and S_u are the area of the remaining ogive-nose surface and the area of the U-shape-nose grooved surface, respectively.

The penetration equation of U-shape-nose grooved projectile motion can be solved by the discretization model with the corresponding partial differential equations transformed into discrete space and time. The deceleration a^i , velocity v^i and displacement Δp^i of projectile during the time step from t^{i-1} to t^i can be expressed as:

$$a^i = \frac{F^i}{m} \tag{24a}$$

$$v^i = v^{i-1} - a^{i-1} \Delta t \tag{24b}$$

$$\Delta p^i = v^{i-1} \Delta t - \frac{a^{i-1} \Delta t^2}{2} \tag{24c}$$

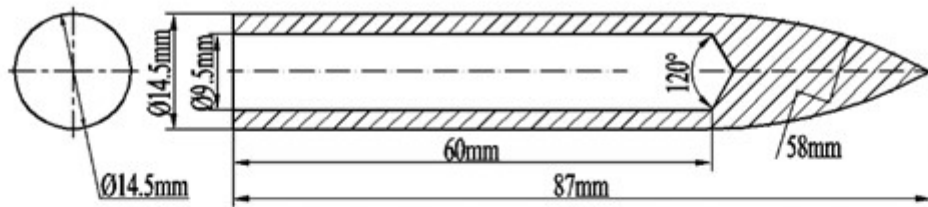
The penetration process of U-shape-nose grooved projectile can be analytically represented with this incremental method, as shown in Figure 6. To guarantee the stability and smooth of the calculation, the time step Δt

should be set small enough as to the whole time of the penetration process. Apparently, the iterative calculation will stop when the instant velocity v get to zero.

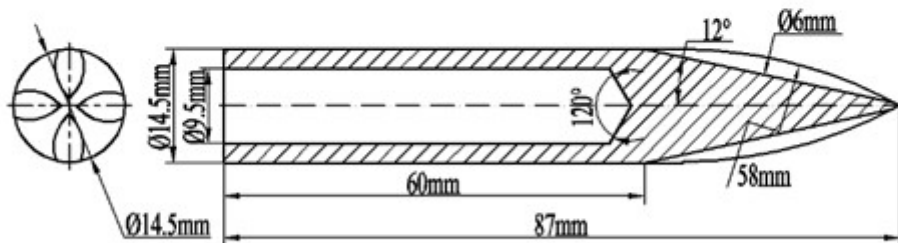
3 PENETRATION EXPERIMENTS OF U-SHAPE-NOSE GROOVED PROJECTILE PENETRATING INTO ALUMINUM TARGET

3.1 Projectile

Comparative penetration experiments were conducted on Ogive-nose projectile and U-shape-nose grooved projectile. In the present test, two series of projectiles with a diameter of 14.5mm, a length of 87mm and an ogive radius of 58mm were used. The hollow structure with a mass of $66g \pm 0.5g$ was used to reduce launch weight in order to satisfy the impact velocity. The projectiles were machined from 30CrMnSi with Rockwell hardness of HRC45 and density of $7790kg/m^3$, respectively. In order to specifically illustrate the geometries of projectiles, the corresponding characteristic parameters are labeled in Figure 7. The U-shape-nose grooved projectile was further processed based on the ogive-nose projectile. According to the parameters definition in Section 2.1, the four geometry parameters (x_0 , α , R_u and n) of U-shape-nose grooved projectile equal 1.6mm, 12° , 6mm and 4, respectively. Figure 8(a) shows the comparative photograph between the ogive-nose projectile and U-shape-nose grooved projectile.



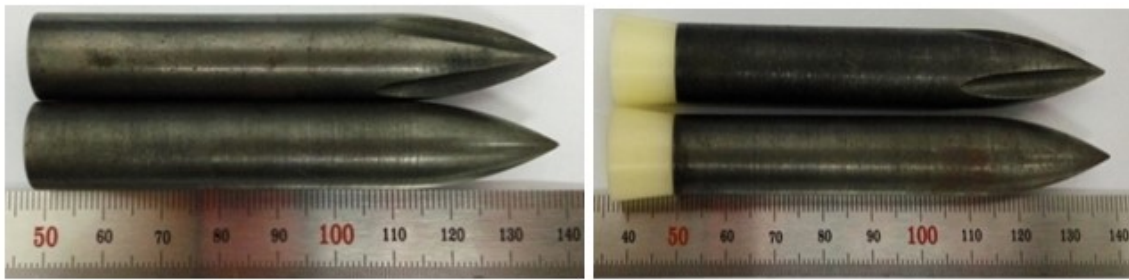
(a) Ogive-nose projectile



(b) U-shape-nose grooved projectile

Figure 7: Schemes of projectiles

As shown in Figure 8(b), both the two series of projectiles were filled by Nylon with the density about $1500kg/m^3$ as inert materials, which was used to stuff in the hole of the projectile to seal propellant gas behind during launching. During each shot, the initial mass of the projectile m was measured and listed in Table 2.



(a) Projectiles (b) Projectiles with obturators

Figure 8: Photograph of projectile

3.2 Target

The material of targets is 2A12 aluminum. To perform the penetration experiments at reasonable costs, the thicknesses of the 2A12 aluminum targets were designed differently according to impact velocities. For high-speed shots (615m/s-793 m/s), the diameter and thickness of the cylindrical targets were 100mm and 120mm, respectively. For low-to-mid speed shots (373m/s-501m/s), targets with thickness of 80mm were supposed to be thick enough, which can be regarded as semi-infinite targets. Besides, the test results are shown in Section 3.4.1 and the targets damages are shown in Section 3.4.2, indicating that the targets in the present tests were thick enough to neglect the boundary effect on the rear face.

The uniaxial compression tests of the 2A12 aluminum were carried out on a static universal testing machine at the strain rate of 10^{-3} s^{-1} . Table 1 lists the material parameters, which includes material density ρ_t , young's modulus E , yield strength Y_t , poisson ratio μ and strain hardening exponent n_t .

Table 1: Material parameters of 2A12

Material	Density ρ_t (kg/m^3)	Young's modulus E (GPa)	Yield strength Y_t (MPa)	Poisson ratio μ	Strain hardening exponent n_t
2A12	2730	69.3	363	0.33	0.069

3.3 Experimental setup

The schematic diagram of the projectile penetration tests is shown in Figure 9. During the tests, the cylindrical targets were placed on their sides, with the longitudinal axis coaxial to the barrel. A steel frame was used to prevent the lateral rolling of the target. Impact velocities were measured from a pair of sensor aluminum foils, which were placed in the straight trajectory of the projectiles between the muzzle and the target. The sensor aluminum foils were connected to a multi-channel velocimeter, forming part of electrical circuits. The time for sequential breakage of the sensor aluminum foils by the projectile was recorded, thus the initial velocity v_0 could be calculated by the distance and the time interval between two sensor aluminum foils. After each shot, the damages of the targets were recorded, including the maximum DOP of the projectiles.

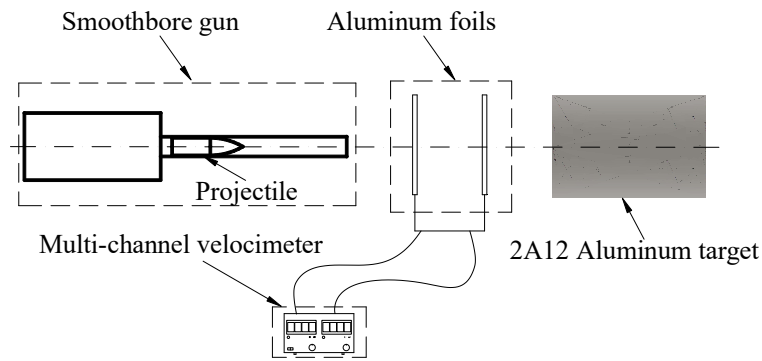


Figure 9: Sketch of projectile penetration test

3.4 Penetration experiment results

3.4.1 Experiments data

In the present tests, projectiles were fired in a range of velocity from 373m/s to 793m/s. Seven shots on 2A12 aluminum target were carried out by ogive-nose and U-shape-nose grooved projectiles, respectively. The experimental results, which include impact velocity v_0 , initial projectile mass m and DOP, are listed in Table 2. It should be noted that the case numbers ONP and USNP represent the experiments with ogive-nose projectile and U-shape-nose grooved projectile, respectively.

Table 2: Experiment data of DOP between ogive-nose projectile and U-shape-nose projectile

Ogive-nose Projectile				U-shape-nose grooved Projectile			
No.	Impact velocity v_0 (m/s)	Mass m (g)	DOP P (mm)	No.	Impact velocity v_0 (m/s)	Mass m (g)	DOP P (mm)
ONP-1	417	65.5	35.6	USNP-1	373	66.3	36.2
ONP-2	501	66.3	41.2	USNP-2	453	66.0	45.1
ONP-3	615	66.4	59.8	USNP-3	615	66.3	67.2
ONP-4	676	65.7	63.5	USNP-4	648	66.2	71.2
ONP-5	719	65.6	73.0	USNP-5	691	66.4	79.2
ONP-6	742	65.6	77.8	USNP-6	745	66.0	89.0
ONP-7	793	65.9	86.4	USNP-7	768	65.7	95.2

3.4.2 Targets damages

Due to the semi-infinite targets, there are no visible bulging or perforated on the rear face of the total 14 targets. The damage views of the impacted faces in each test are shown in Figure 10, respectively. Damages on the 2A12 aluminum targets are always accompanied by the phenomenon of the extrusion of target material after penetration by the U-shape-nose grooved projectile. Figure 11 illustrates the typical photographs of the extrusion of the target material.

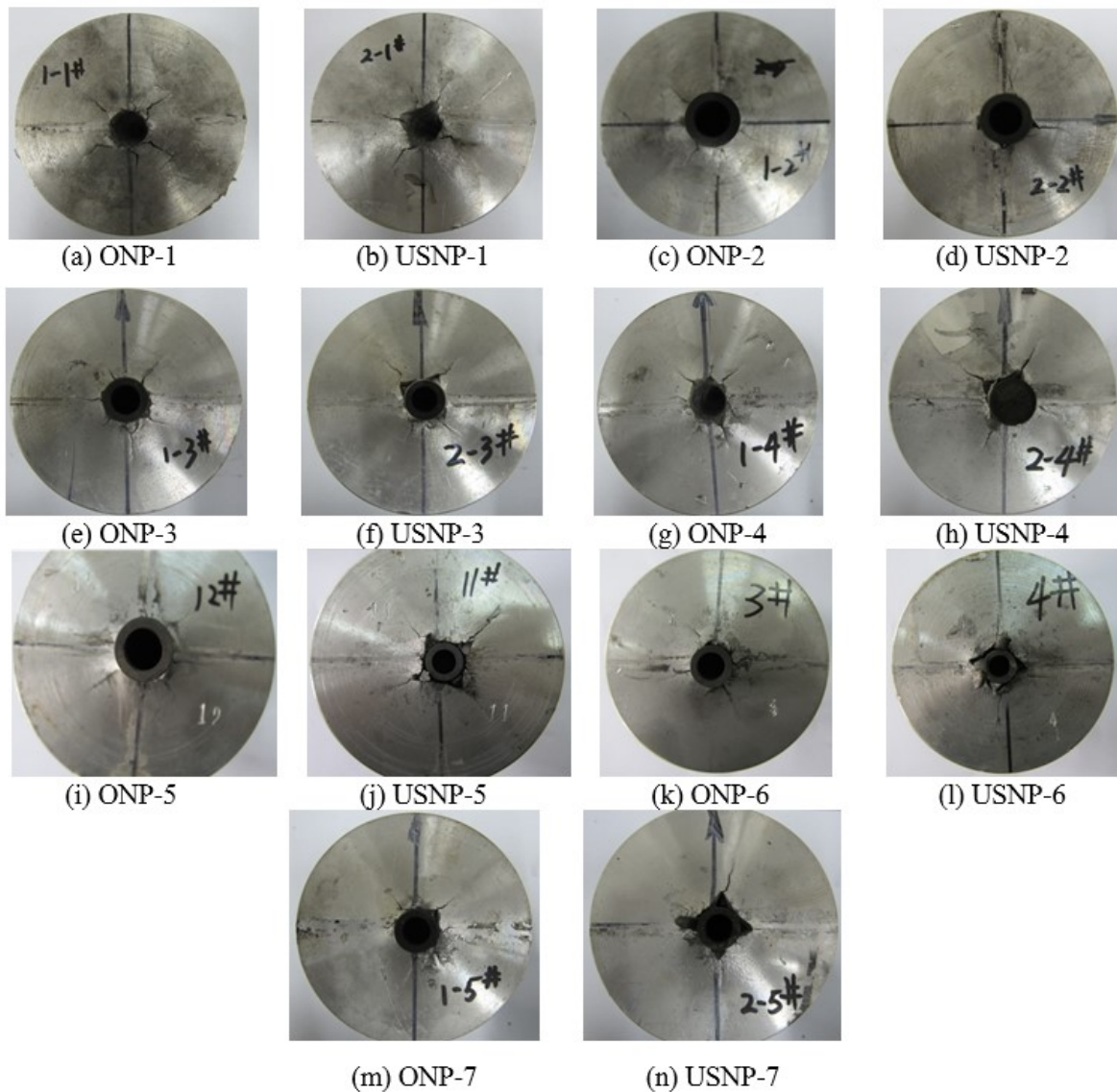


Figure 10: Targets damages

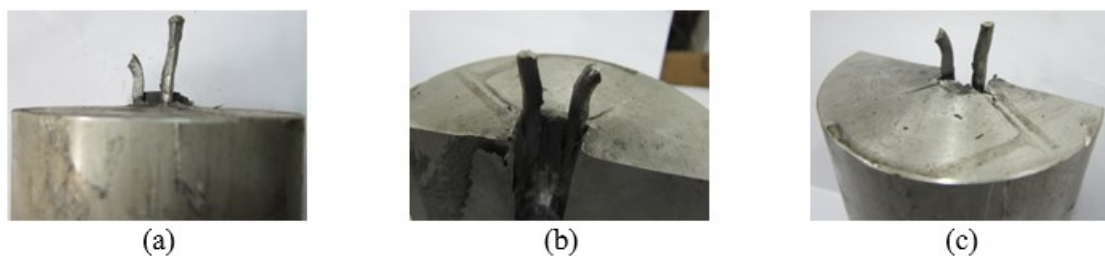


Figure 11: Phenomenon of target material extrusion of USNP-7

3.4.3 Terminal ballistic trajectory

During all the penetration tests, the penetration paths of projectiles were all straight. Figure 12 illustrated the terminal ballistic trajectories in partial tests (ONP-5, USNP-5, ONP-7, USNP-7) obtained by cutting the targets after shots.

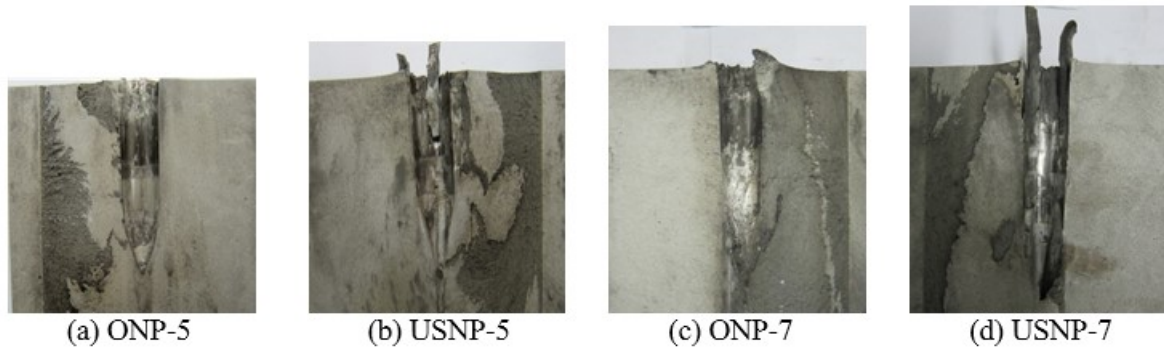


Figure 12: Terminal ballistic trajectories obtained by cutting the targets

3.5 Analysis of penetration results

3.5.1 Characteristic analysis of targets damages

The structure of projectile, especially the nose of the projectile, affects the penetration performance of the projectile. The essence of the variation in penetration performance is the change in the form of the target damage during the penetration. Thus, the mechanism of target damage caused by U-shape-nose grooved projectile is investigated through characteristic analysis in this section.

Commonly, the hole of the target produced by ogive-nose projectile (Figure 10(a), (c), (e), (g), (i), (k), (m)) is cylinder, along with the upheaved of target material on the impacted face of target. Meanwhile, 5-7 cracks uniformly distribute and extend away from the edge of the hole. According to the target damages by U-shape-nose grooved projectiles in Figure 10, the hole of the target is an approximate cylinder with four sharp angles. The positions to generate sharp angles is corresponding to the relative positions of U-shape-nose surfaces of the projectile during the penetration. Different from the crack of the targets from the penetration of ogive-nose projectile, there are only four cracks appearing at the tip of the sharp angles and extending to the target boundary. The phenomenon of appearing sharp angle increases significantly with the increase of impact velocity. As shown in Figure 11 and Figure 12(b-d), the target material is extruded as the shape of banded chip at the penetration position of the U-shape-nose grooved surface. Moreover, four banded chips of the target material flow along the opposite penetration direction with the further penetration of projectile. Therefore, the sharp angle appears around the impacted face, while the groove shape was produced in the terminal ballistic trajectory.

Compared with the traditional characteristic of the target damage, the U-shape-nose grooved projectile produces irregular impacted surface hole and terminal ballistic trajectory. The extrusion of the target material appears in the penetration process, which can be regarded as the removal of the chip. The nose of the U-shape-nose and ogive-nose projectile compress the target material around the contact surface between the target and projectile at the beginning of the penetration process. Due to the favorable ductility of 2A12 aluminum, the material is extruded and forms the long banded chips along the U-shape-nose grooved surface of the projectile. The long banded chips flow out from the impact face of the target with the motion of a projectile, resulting in the cylindrical hole with four sharp angles at the impacted surface. During the penetration of U-shape-nose grooved projectile into the target, the stress concentration at the sharp angle of the hole increases with the compression of the target. Under the high compression, the tip of the sharp angle is torn and generates the crack. When the U-shape-nose grooved surface of the projectile fully immerses into the target, the target material is no longer extruded and the failure mode of the target transform into the form of the unitary compression damage.

3.5.2 Analysis of DOP by projectile of different nose shape

Generally, the penetration performance of the projectile is mainly presented by the ultimate DOP. In order to evaluate the penetration performance of U-shape-nose grooved projectile, the comparison of DOP between the traditional ogive-nose projectile and the U-shape-nose grooved projectile is conducted in this chapter. As shown in Figure 13, the quadratic polynomial curve of DOP-initial velocity relationship is fitted by the data in Table 2. By comparing the shots ONP-1, ONP-2, USNP-1, and USNP-2, as well as the initial velocity ranging from 300m/s to 500m/s in the quadratic polynomial fitting curve, the increase rate of DOP of the U-shape-nose grooved projectiles significantly increases with the increasing initial velocity. It indicates that the DOP was increased with the U-shape-nose groove of the projectile, of which the increase degree tends to be constant with the initial impact velocity from 500m/s to 800m/s.

It can be found that projectile with U-shape-nose grooves realizes the sharpening effect during the penetration process. The appearance of sharp angle and the subsequent crack in the target changes the stress distribution around the surface of projectile. The phenomenon of the chip removal appears on the U-shape grooved arc surface, which decreases the target area of unitary compressed damage. The experimental results prove that the projectile with U-shape-nose grooves plays an essential role in reducing the penetration resistance and enhancing DOP.

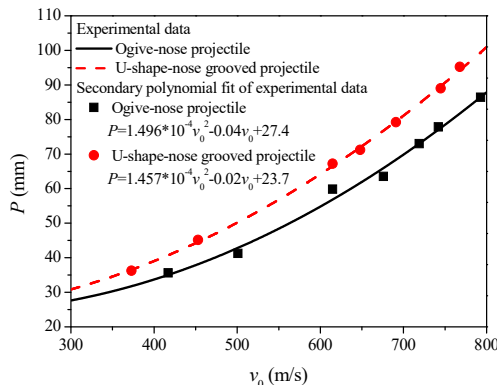


Figure 13: Experimental data and fitting curves of DOP

4 DISCUSSIONS ON THE THEORETICAL MODEL

4.1 Validation of theoretical predictions with experimental results

In order to validate the proposed penetration depth equation, the calculation results are compared with the experiment data. The experimental DOP and corresponding theoretical predictions of the ogive-nose projectile into 2A12 aluminum target are listed in Table 3. It is clear that the theoretical prediction of ogive-nose projectile is almost consistent with the experiment data. As shown in Table 3, the theoretical prediction of DOP for U-shape-nose grooved projectile is lower than experiment results, the average deviation of which is about 9.19%. The penetration depth equation based on the Localized Interaction models takes into account the sharpening effect of the U-shape-nose grooved projectile, which is suitable to predict the DOP of U-shape-nose grooved projectile into a ductile metal target. The reason for the relatively large deviation is that the current analysis model neglects the variation of the cavity expansion stress and the phenomenon of the chip removal. Compared with DOP of ogive-nose projectile, the sharpening effects of the U-shape-nose grooved projectile lead to the slight increase of DOP in the calculation of analytical model. The relative deviation proves that the main reason for the increase of DOP is the change in failure mode of the target and the reduction of the penetration resistance but not merely the sharpening effect.

Table 3: Contrast between theoretical predication and experiment result

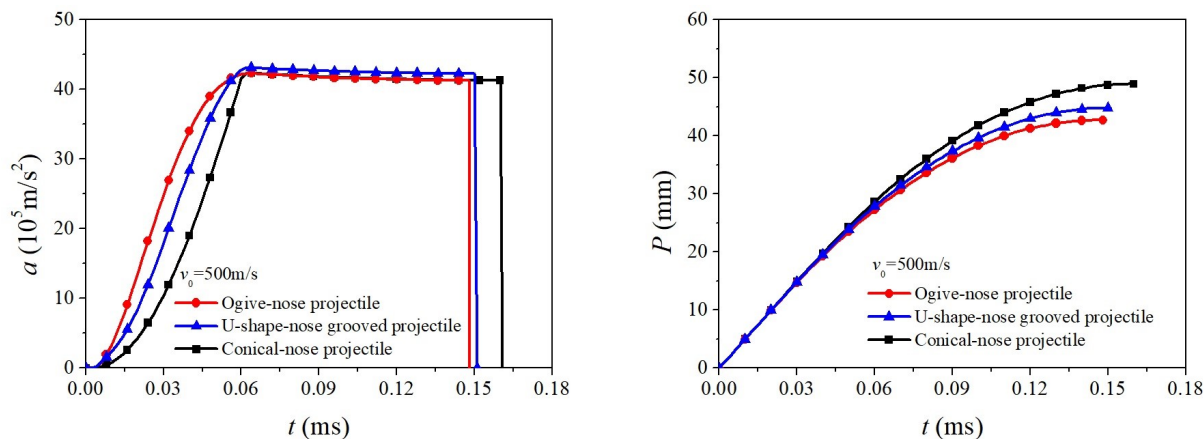
Projectile type	No.	Impact velocity v_0 (m/s)	Experimental DOP (mm)	Theoretical DOP (mm)	Relative deviation (%)
Ogive-nose projectile	ONP-1	417	35.6	33.8	5.06
	ONP-2	501	41.2	42.8	3.88
	ONP-3	615	59.8	57.4	4.01
	ONP-4	676	63.5	66.2	4.25
	ONP-5	719	73.0	72.8	0.27
	ONP-6	742	77.8	76.5	1.67
	ONP-7	793	86.4	85.0	1.62
U-shape-nose grooved Projectile	USNP-1	373	36.2	33.3	8.01
	USNP-2	453	45.1	41.0	9.09
	USNP-3	615	67.2	60.7	9.67
	USNP-4	648	71.2	65.4	8.15
	USNP-5	691	79.2	71.8	9.34
	USNP-6	745	89.0	81.4	8.54
	USNP-7	768	95.2	84.2	11.55

4.2 Penetration of U-shape-nose grooved projectile

The penetration performance of U-shape-nose grooved projectile is further investigated by utilizing the discretization model of penetration equation of projectile motion in Section 2.3. General ogive-nose projectile and conical-nose projectile, as well as the U-shape-nose grooved projectile, are selected to comparatively analyze the penetration process. Three types of the projectiles are all assumed to be rigid with the same nose length and a same initial kinetic energy. The length, radius, ogive-nose radius and nose length of the projectile are as same as the geometrical dimensions in Figure 6(a). The length of the U-shape-nose groove is $L_u=b-x_0$, which represents that the grooves exist only on the nose surface of the U-shape-nose grooved projectile.

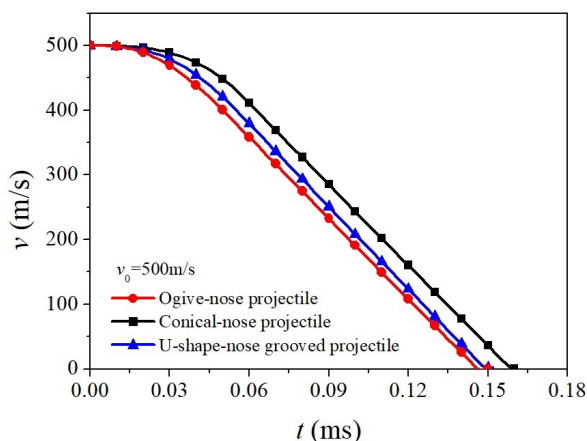
The time-history curves of the penetration process, including the deceleration time history, depth of penetration time history and time history, are shown in Figure 14. It is clear that the conical-nose projectile has the lower deceleration, slower attenuation of velocity and larger depth of penetration than the other projectiles. Compared with the ogive-nose projectile, the U-shape-nose grooved projectile shows a more slowly increasing deceleration at the beginning penetration stage and a higher smooth deceleration at the stable penetration stage. Besides, the U-shape-nose grooved projectile has a larger peak of deceleration value and wider pulse than the ogive-nose projectile, which results in the increase of depth of penetration. It is reasonable to explain that the conical-nose projectile is fully nose sharpening projectile. On the other side, the groove on the U-shape-nose grooved projectile can be regarded as partial sharpening from the ogive-nose, the resistance of which is between the ogive-nose projectile and conical-nose projectile.

The calculated results prove that U-shape-nose grooved projectile is subjected to a relatively small penetration resistance. Therefore, the grooved nose shape makes a major contribution to enhance DOP.



(a) Deceleration time history curves

(b) Depth of penetration time history curves



(c) Velocity time history curves

Figure 14: Calculated time-history curves for three projectiles

4.3 Characteristic parameters analysis of the U-shape-nose grooved projectile

Regardless of target damage, the influence factors on the penetration performance include four characteristic parameters of the U-shape-nose grooved projectile (n , R_u , x_0 , α). The effect of each characteristic parameter on the dimensionless DOP (the ratio of DOP of U-shape-nose grooved projectile to DOP of the ogive-nose projectile) is theoretically analyzed in this section. The geometrical dimensions of projectiles, which are used in the theoretical calculation, are the same with the case in Section 4.2.

The nose of projectile tends to be more sharpened with the increasing number of groove n . As shown in Figure 15(a), the dimensionless DOP increases in a nearly linear relationship as the number of the groove increased, while the slopes of the curves become relatively flattered with the impact velocity increases. The area, depth, and length of U-shape-nose groove are controlled by the X-coordinate value (x_0) of initial groove position. Figure 15(b) shows the dimensionless DOP and the value of x_0 under different impact velocity. The figure shows that the dimensionless DOP increases with initial groove position closer to the tip of the projectile. Due to lacking of groove on the projectile surface when $x_0 \geq b$, the projectile becomes to be the ogive-nose projectile. According to the penetration depth equation, the reduction of x_0 results in the increase of 2γ in the range of 0 to $2\pi/n$. The radius of U-shape-nose groove R_u influences the area of single groove and the position relationship between every two grooves. As shown in Figure 15(c), the DOP of the U-shape-nose grooved projectile is significantly lower than the ogive-nose projectile, where the radius of U-shape-nose groove is smaller. Furthermore, the dimensionless DOP is higher than 1 and increase with the growth of the radius of U-shape-nose groove when the radius of U-shape-nose groove is larger enough. It indicates that, without increasing the resistance area on the projectile surface, the U-shape-nose groove effectively reduces the area of the original ogive-nose surface and then influences the resistance during penetration and the ultimate DOP. The angles of U-shape-nose groove α affects DOP, the terminal position and the length of U-shape-nose groove. From Figure 15(d), the dimensionless DOP increases with decrease value of α . The decrease of α results in the increase of the length and depth of the U-shape-nose groove, which increases the U-shape-nose groove surface area and finally influences the ultimate DOP.

Based on the above-mentioned analysis, the essence of parameter variation is to realize sharpening of the projectile by increasing the area of the U-shape-nose grooved surface. With the decrease of ogive-nose arc surface and the increase of U-shape-nose grooved arc surface, the U-shape-nose grooved projectile has lower penetration resistance and more excellent penetration capability. However, sharpening effect of the U-shape-nose groove weakens as impact velocity increases.

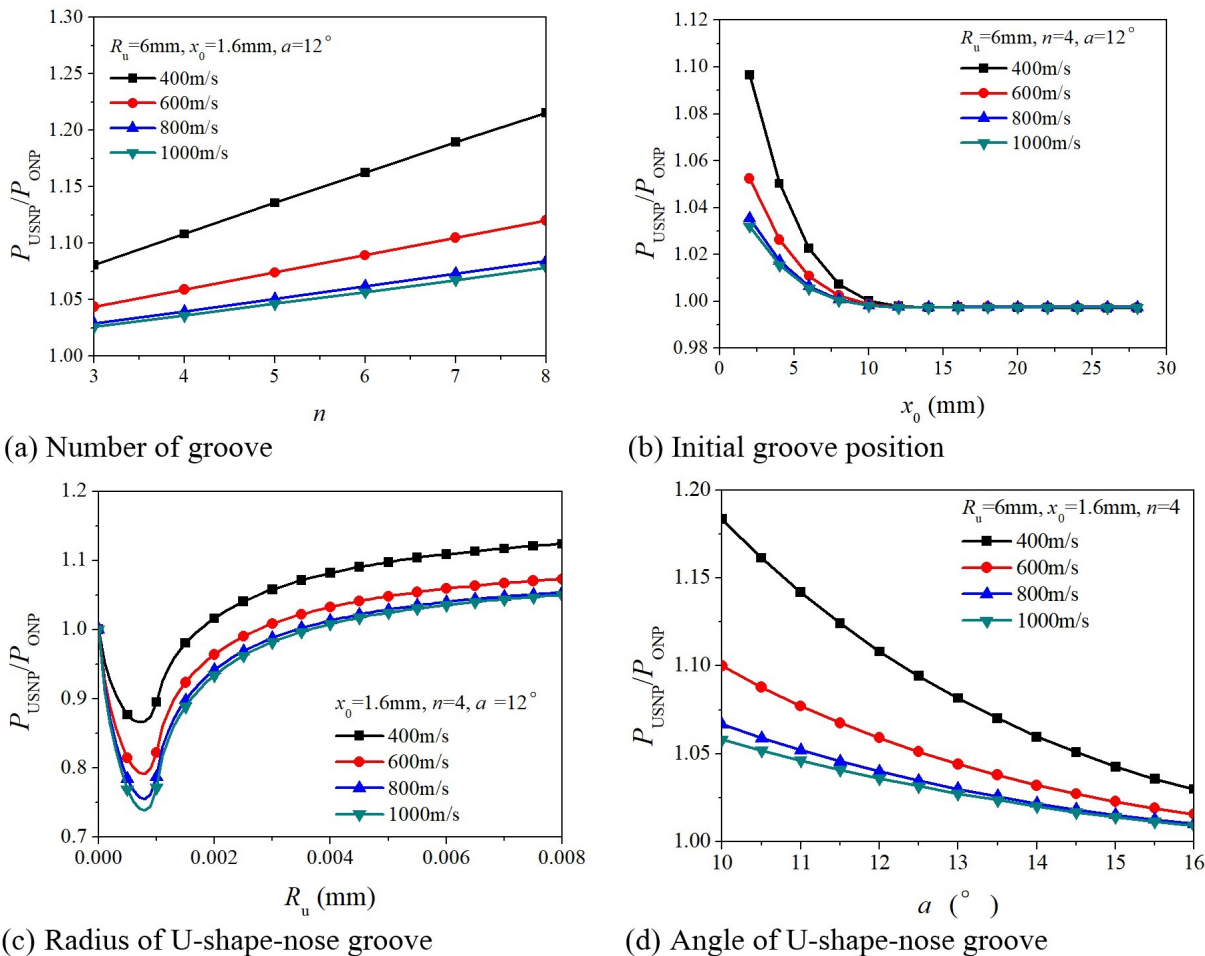


Figure 15: Dimensionless DOP versus nose-shape parameters of U-shape-nose grooved projectile

5 CONCLUSION

Based on the structural characterization of U-shape-nose grooved projectile, an analytical model is constructed to investigate the depth of penetration and penetration process of U-shape-nose grooved projectile into a ductile metal target. To further study the penetration performance, comparative penetration experiments were conducted on the ogive-nose projectile and U-shape-nose grooved projectile. Characteristic parameters of the U-shape-nose grooved projectile on the penetration performance are analyzed and discussed based on the analytical model which is validated by the experimental results.

The comparison results of experimental DOP demonstrate excellent penetration performance of U-shape-nose grooved projectile. Furthermore, the phenomenon of the chip removal and the cylindrical hole with four sharp angles can be observed in the target impacted by U-shape-nose grooved projectile. The flow direction of the target material, the shape of trajectory and number of crack on the impacted face are different from the damage mode of traditional target. It indicates that the projectile with U-shape-nose groove causes the variation of target damage mode during the penetration.

The DOPs of U-shape-nose grooved projectile, which calculated by analytical model, are compared with the experimental data. The comparison show that the main factor to increase the DOP is the variation of failure mode of the target but not merely the sharpening effect. The analysis of characteristic parameters, DOP, and penetration process proves that the U-shape-nose grooved projectile increases DOP to sharpen the projectile while U-shape-nose grooved projectile is subjected to a relatively small penetration resistance.

In summary of the experimental and theoretical analysis, U-shape-nose grooved projectile reveals a more excellent penetration performance than the ogive-nose projectile. The analytical model of U-shape-nose grooved projectile into ductile metal target shows good predictability and practicability, which can be used to the prediction of DOP and optimal design of U-shape-nose grooved projectile. The resistance characteristics of U-shape-nose

grooved projectile impacting on ductile metal target, as well as the research on the brittle target should be performed in the future.

Acknowledgements

This research is supported by the National Program for Support of Top-notch Young Professionals of China, the Fundamental Research Funds for the Central Universities (No. 30916011305), and the National Natural Science Foundation of China (NSFC U1730101). The authors would also like to thank, Dr. Chunxu Pang, Mr. Fei Gao, Mr. Dongdong Chen, and Mr. Yang Wu for their great support on the current experimental work.

References

Ben-Dor G., Dubinsky A., Elperin T., (1996). Applied high-speed plate penetration dynamics. Springer, Netherlands.

Ben-Dor G., Dubinsky A., Elperin T., (2009). High-Speed Penetration Modeling and Shape Optimization of the Projectile Penetrating into Concrete Shields. *Mechanics based design of structures and machines* 37(4):538-549.

Bishop R. F., Hill R., Mott N. F., (1945). The theory of indentation and hardness tests. *Proceedings of the Physical Society* 57(3):147.

Chai C. G., (2014) Study on the mechanism of penetration into concrete of nose headed projectile, Ph.D. Thesis (in Chinese), Beijing Institute of Technology, China.

Chen X. W., Li Q. M., (2002). Deep penetration of a non-deformable projectile with different geometrical characteristics. *International Journal of Impact Engineering* 27(6): 619-637.

Dubinskii A. V., (1995). Mathematical models and methods of localized interaction theory. World Scientific, Singapore.

Erengil M. E., Cargile D. J., (2002) Advanced projectile concept for high speed penetration of concrete targets. *Proceedings of 20th International Symposium on Ballistics*, Orlando.

Fan S. B., Chen Z. G., Hou X. C., et al., (2013). Numerical simulation and experimental study on novel rotating penetration projectile[J]. *Journal of Projectiles, Rockets, Missiles and Guidance* (1):80-83. (in Chinese)

Forrestal M. J., Altman B. S., Cargile J. D., et al., (1994). An empirical equation for the penetration depth of ogive-nose projectiles into concrete targets. *International Journal of Impact Engineering* 15(4):395-405.

Forrestal M. J., Warren T. L., (2008). Penetration equations for ogive-nose rods into aluminum targets. *International Journal of Impact Engineering* 35(8):727-730.

Guo J., Pan X. C., He Y., et al., (2015). Study on the influence of projectile shape on rotary penetration depth of concrete target. *Journal of ballistics* 27(2): 74-79. (in Chinese)

Hatami H., Nouri M. D., (2015). Experimental and numerical investigation of lattice-walled cylindrical shell under low axial impact velocities. *Latin American Journal of Solids and Structures* 12(10): 1950-1971.

Hatami H., Rad M. S., Jahromi A. G., (2017). A theoretical analysis of the energy absorption response of expanded metal tubes under impact loads. *International Journal of Impact Engineering* 109: 224-239.

He L. L., Chen X. W., Wang Z. H., (2016). Study on the penetration performance of concept projectile for high-speed penetration (CPHP). *International Journal of Impact Engineering* 94:1-12.

Hill R., (1980). Cavitation and the influence of headshape in attack of thick targets by non-deforming projectiles. *Journal of the Mechanics and Physics of Solids* 28(5-6):249-263.

Jahromi A. G., Hatami H., (2017). Energy absorption performance on multilayer expanded metal tubes under axial impact. *Thin-Walled Structures* 116: 1-11.

Jones S. E., Rule W. K., (2000). On the optimal nose geometry for a rigid penetrator, including the effects of pressure-dependent friction. *International journal of impact engineering* 24(4): 403-415.

Li Q. M., Chen X. W., (2003). Dimensionless formulae for penetration depth of concrete target impacted by a non-deformable projectile. *International Journal of Impact Engineering* 28(1): 93-116.

Li Y. C., Sun Y. X., Hu X. Z., et al, (2000). A new engineering analytical method on concrete anti-penetration. *Explosion and Shock Waves* 20(1):13-18. (in Chinese)

Liang B., Chen X., Ji Y., et al., (2008). Experimental study on deep penetration of reduced-scale advanced earth penetrating weapon. *Explosion and Shock Waves* 28(1):1. (in Chinese)

Liu J. C., Huang F. L., Pi A. G., et al., (2014). On enhanced penetration performance of modified nose projectiles. *Explosion and Shock Waves* 34(4): 409-414. (in Chinese)

Liu J., Pi A., Huang F., (2015). Penetration performance of double-ogive-nose projectiles. *International Journal of Impact Engineering* 84:13-23.

Luk V. K., Forrestal M. J., (1987). Penetration into semi-infinite reinforced-concrete targets with spherical and ogival nose projectiles. *International Journal of Impact Engineering* 6(4):291-301.

Luk V. K., Forrestal M. J., Amos D. E., (1991). Dynamic spherical cavity expansion of strain-hardening materials. *Journal of Applied mechanics* 58(1):1-6.

Mayersak J., (2003) Kinetic energy cavity penetrator weapon: U.S. Patent Application 10/443,621.

Nouri M. D., Hatami H., (2017). Experimental and numerical study of the effect of longitudinal reinforcements on cylindrical and conical absorbers under impact loading. *Indian Journal of Science and Technology* 7(2): 199-210.

Nouri M. D., Hatami H., Jahromi A. G., (2015). Experimental and numerical investigation of expanded metal tube absorber under axial impact loading. *Structural Engineering & Mechanics* 54(6): 1245-1266.

Pang C. X., He Y., Shen X. J., et al., (2015a). Experimental investigation and numerical simulation on grooved projectile rotationally penetration into aluminum target. *Journal of Ballistics* (1):70-75. (in Chinese)

Pang C. X., He Y., Shen X. J., et al., (2015b). Experimental investigation on penetration of grooved projectiles into concrete targets. *Acta armamentarii* 36(1):46-52. (in Chinese)

Piekutowski A. J., Forrestal M. J., Poormon K. L., et al., (1996). Perforation of aluminum plates with ogive-nose steel rods at normal and oblique impacts. *International Journal of Impact Engineering* 18(7-8): 877-887.

Ragnedda F., Serra M., (2010). Optimum shape of high speed impactor for concrete targets using PSO heuristic. *Engineering* 2(04):257.

Wu H., Wang Y., Huang F., (2008). Penetration concrete targets experiments with non-ideal & high velocity between 800 and 1100m/s. *International Journal of Modern Physics B* 22(09n11):1087-1093.

- Yakunina G. Y., (2001). Optimum three-dimensional hypersonic bodies within the framework of a local interaction model. *AIAA Paper (2001-1797)*:11.
- Yakunina G. Y., (2005). The three-dimensional motion of optimal pyramidal bodies. *Journal of applied mathematics and mechanics* 69(2):234-243.
- Yakunna G Y., (2005). Effects of sliding friction on the optimal 3D-nose geometry of rigid rods penetrating media. *Optimization and Engineering* 6(3):315-338.
- Yankelevsky D Z, (1997). Local response of concrete slabs to low velocity missile impact. *International journal of impact engineering* 19(4):331-343.
- Yankelevsky D. Z., Adin M. A., (1980). A simplified analytical method for soil penetration analysis. *International Journal for Numerical and Analytical Methods in Geomechanics* 4(3):233-254.
- Yankelevsky D. Z., Gluck J., (1980). Nose shape effect on high velocity soil penetration. *International Journal of Mechanical Sciences* 22(5): 297-311.
- Zhang S., Wu H., Zhang X. X. et al., (2017). High-velocity Penetration of Concrete Targets with Three Types of Projectiles: Experiments and Analysis. *Latin American Journal of Solids and Structures* 14(09):1614-1628.
- Zhang X. X., Wu H. J., Huang F. L., et al., (2014). An Investigation on the Grooved-tapered Projectile Penetrating into the Concrete Targets. *Applied Mechanics and Materials. Trans Tech Publications* 566: 359-364.
- Zhang, X. X., (2016). The response characteristic of high-speed grooved tapered projectile penetrating into the concrete, Ph.D. Thesis (in Chinese), Beijing Institute of Technology, China.
- Zhang, X. X., Yan, L., Wu, H. J., Huang, F. L., (2016). A note on the dynamic spherical cavity expansion of concrete with shear dilatancy. *Binggong Xuebao/acta Armamentarii* 37(1):42-49. (in Chinese)
- Zhao J., Chen X. W., Jin F. N., et al, (2003). Depth of penetration of high-speed penetrator with including the effect of mass abrasion. *International Journal of Impact Engineering* 37(9): 971-979.